One-Atom-Thick IR Metamaterials and Transformation Optics Using Graphene

Ashkan Vakil and Nader Engheta*

University of Pennsylvania

Department of Electrical and Systems Engineering

Philadelphia, Pennsylvania 19104, U.S.A.

Abstract

Here we theoretically show, by designing and manipulating *spatially inhomogeneous*, *non-uniform* conductivity patterns across a single flake of graphene, that this single-atom-layered material can serve as a "one-atom-thick" platform for infrared metamaterials and transformation optical devices. It is known that by varying the chemical potential using gate electric and/or magnetic fields, the graphene conductivity in the THz and IR frequencies can be changed. This versatility provides the possibility that different "patches" on a single flake of graphene possess different conductivities, suggesting a mechanism to construct "single-atom-thick" IR metamaterials and transformation optical structures. Our computer simulation results pave the way for envisioning numerous IR photonic functions and metamaterial concepts—all on a "one-atom-thick" platform—of such we list a few here: edge waveguides, bent ribbon-like paths guiding light, photonic splitters and combiners, "one-atom-thick" IR scattering elements as building blocks for 'flatland' metamaterials, thin strips as flatland superlenses, and "one-atom-thick" subwavelength IR lenses as tools for Fourier and transformation optics.

* To whom correspondence should be addressed. E-mail: engheta@ee.upenn.edu

The fields of plasmonics, metal optics, metamaterials and transformation optics *(1-7)* have received considerable attention in recent years, since they offer a variety of schemes to manipulate electromagnetic fields into desired spatial patterns, suggesting exciting potential applications in various branches of engineering and applied science. Owing to their ability to support the surface-plasmon polariton (SPP) surface waves *(8)* in the infrared and visible regimes, the noble metals, such as silver and gold, have been popular constituent materials for constructing optical metamaterials *(1)*. From the macroscopic electromagnetic view point, the plasmonic characteristics are associated with the noble metals permittivity function exhibiting negative real part *(8)*. However, the difficulty in controlling and varying permittivity functions of the noble metals and the existence of material losses in them—especially at visible wavelengths—degrade the quality of the plasmon resonance and limit the relative propagation lengths of SPP waves along such metal-dielectric interfaces. These drawbacks, therefore, constrain the functionality of some of metamaterials and transformation optical devices. It is, therefore, laudable to search for new suitable materials for these purposes.

In recent years, there has been an explosion of interest in the field of graphene, which has exciting properties in electronic transport *(9-24)*. An important parameter in describing optical characteristics of graphene is the complex conductivity $\sigma_g = \sigma_{g,r} + i\sigma_{g,i}$, which depends on radian frequency ω, charged particle scattering rate Γ representing loss mechanism, temperature T, and chemical potential μ_c.The chemical potential depends on the carrier density and can be controlled by a gate voltage, electric field, magnetic field and/or chemical doping *(11-20)*. One of the interesting properties of graphene is that the imaginary part of its conductivity, i.e., $\sigma_{g,i}$, can, under certain conditions, attain negative and positive values in different ranges of

frequencies depending on the level of chemical potential *(13)*. Figures 1a and b depict the real and imaginary parts of the conductivity of a free-standing isolated graphene as a function of frequency and chemical potential, computed from the Kubo formula with $T = 3\text{K}$ and $\Gamma = 0.43\,\text{meV}$ 11, 13 (μ_c up to 400 meV and the frequency range of 10 to 50 THz). As can be seen, there are regions of frequencies and chemical potentials (or gate voltages) for which $\sigma_{g,i} < 0$, while in other regions $\sigma_{g,i} > 0$.

What is the significance of $\sigma_{g,i}$ attaining positive or negative values in the context of metamaterials? To address this issue, we momentarily assume that graphene has a very small thickness Δ (Later we shall let $\Delta \to 0$). We point out that it is possible to associate an *equivalent* complex permittivity for this Δ-thick graphene layer. Defining a *volume* conductivity for this Δ-thick graphene layer as $\sigma_{g,v} \equiv \frac{\sigma_g}{\Delta}$, we can then write its *volume* current density as $\boldsymbol{J} = \sigma_{g,v}\boldsymbol{E}$. Assuming $\exp(-i\omega t)$ time harmonic variations, we can rearrange the Maxwell equation $\nabla \times \boldsymbol{H} = \boldsymbol{J} - i\omega\varepsilon_o\boldsymbol{E}$ for the Δ-thick graphene layer as $\nabla \times \boldsymbol{H} = (\sigma_{g,v} - i\omega\varepsilon_o)\boldsymbol{E}$. Denoting the *equivalent* complex permittivity of the Δ-thick graphene layer by $\varepsilon_{g,eq}$, we obtain $\varepsilon_{g,eq} \equiv -\frac{\sigma_{g,i}}{\omega\Delta} + \varepsilon_o + i\frac{\sigma_{g,r}}{\omega\Delta}$. We realize that for a one-atom-thick layer, one cannot define any bulk permittivity. However, here we have temporarily assumed that the thickness of layer is Δ, associating an equivalent permittivity with this single layer. This approach allows us to treat the graphene sheet as a thin layer of material with $\varepsilon_{g,eq}$. At the end we let $\Delta \to 0$, and recover the one-atom-thick layer geometry. Specifically, we note that $\text{Re}(\varepsilon_{g,eq}) \equiv -\frac{\sigma_{g,i}}{\omega\Delta} + \varepsilon_o \approx -\frac{\sigma_{g,i}}{\omega\Delta}$ for a

very small Δ, and $\mathrm{Im}(\varepsilon_{g,eq}) \equiv \frac{\sigma_{g,r}}{\omega\Delta}$. This interestingly shows that the real part of equivalent permittivity for this Δ-thick graphene layer can be positive or negative depending on the sign of the imaginary part of the graphene conductivity. Therefore, when $\sigma_{g,i} > 0$, i.e., $\mathrm{Re}(\varepsilon_{g,eq}) < 0$, a single free-standing layer of graphene does effectively behave as a very thin "metal" layer, capable of supporting a transverse-magnetic (TM) electromagnetic SPP surface wave. Other groups have also predicted the possibility of existence of SPP along the graphene *(13-16, 22)*; however, here we present a different method to highlight this feature.

It is known that a slab of a material with complex permittivity ε_m with negative real part (e.g., Ag or Au) and with thickness Δ, surrounded by free space can support an odd transverse-magnetic (TM) electromagnetic guided mode with wave number β expressed as (25)

$$\coth\left(\sqrt{\beta^2 - \omega^2\mu_o\varepsilon_m}\;\Delta/2\right) = -\frac{\varepsilon_m}{\varepsilon_o}\frac{\sqrt{\beta^2 - \omega^2\mu_o\varepsilon_0}}{\sqrt{\beta^2 - \omega^2\mu_o\varepsilon_m}}. \qquad (1)$$

By substituting ε_m with the equivalent permittivity of the Δ-thick graphene layer derived above, and letting $\Delta \to 0$, we get $\beta^2 = k_0^{\,2}\left[1 - \left(\frac{2}{\eta_0\sigma_g}\right)^2\right]$, which is the dispersion relation of the TM SPP optical surface wave along a graphene layer obtained by several groups *(13-16)*. However, when $\sigma_{g,i} < 0$ (i.e., when $\mathrm{Re}(\varepsilon_{g,eq}) > 0$) TM guided surface wave is no longer supported on the graphene *(13-16)*. Instead a weakly guided transverse-electric (TE) surface wave might be present (13-14). Figures 1c and 1d present also the complex wave number β for such TM SPP, as a function of frequency and chemical potential for $T = 3\,\mathrm{K}$ and $\Gamma = 0.43\,\mathrm{meV}$. The

quantity $\mathrm{Re}(\beta)/\mathrm{Im}(\beta)$, which is known as figure-of-merit, and the propagation length $1/\mathrm{Im}(\beta)$ are also shown in Figs. 1e and 1f.

By comparing the graphene with a thin layer of noble metal such as Silver or Gold, one may count at least three major advantages for a graphene layer: 1) In the mid infrared (IR) wavelengths, the "loss tangent" in graphene at low temperatures can be much lower than in silver or gold at room temperature. For example, for a free-standing graphene at $T = 3\mathrm{K}$, $\Gamma = 0.43\,\mathrm{meV}$, and the chemical potential $\mu_c = 0.15\ \mathrm{eV}$ for a signal with the frequency 30 THz, the ratio of $\sigma_{g,r}/|\sigma_{g,i}|$, which is equivalent of $\mathrm{Im}(\varepsilon_{g,eq})/|\mathrm{Re}(\varepsilon_{g,eq})|$, is about 1.22×10^{-2}. On the other hand, this parameter for silver *(26)* at 30 THz at room temperature is about 5.19×10^{-1}; 2) As can be seen in Fig. 1c, the real part of wave number β for the TM SPP wave along the graphene is much larger than the wave number of the free space, $k_o \equiv \omega\sqrt{\mu_o\varepsilon_o}$. As a result, such a SPP wave is very tightly confined to the graphene layer, with guided wavelength λ_{SPP} much shorter than free space wavelength λ_o, i.e., $\lambda_{SPP} << \lambda_o$, consistent with Ref *(16)*. For a layer of graphene with above characteristics, we have $\mathrm{Re}(\beta) = 69.34k_o$ and $\mathrm{Im}(\beta) = 0.71k_o$, resulting an impressive figure of merit of $\mathrm{Re}(\beta)/\mathrm{Im}(\beta) = 97.7$; 3) arguably, the most important advantage of graphene over thin metal layers is the ability to dynamically tune the conductivity of graphene by means of chemical doping or gate voltage, i.e., E_{bias} in real time, locally and inhomogeneously. In other words, by using different values of E_{bias} at different locations across the single graphene layer, in principle we can create certain desired conductivity pattern. We mentioned that at a given frequency a proper choice of chemical potential (or equivalently gate electric biasing field E_{bias}) can provide us with $\sigma_{g,i} > 0$ or $\sigma_{g,i} < 0$. Since the conductivity is directly related to

the equivalent permittivity for the Δ-thick graphene layer as described above, the conductivity variation results in variation of equivalent permittivity across the single sheet of graphene. This provides an exciting possibility for tailoring and manipulating infrared SPP waves across the graphene layer. Therefore the graphene can be considered as a single-atom-thick platform for manipulation of IR signals, providing a "flatland" paradigm for IR metamaterials and transformation optics. In the rest of this Letter, we present several scenarios in which the proper choice of IR conductivity spatial patterns across the graphene provides exciting novel possibilities for tailing, manipulating, and scattering IR guided wave signals on the graphene. These scenarios can be a starting point for having flatland metamaterials and "one-atom-thick" transformation optical devices with exciting functionalities.

To start, consider the numerical simulation of the SPP mode at 30 THz guided by a uniformly biased graphene layer in Fig. 2a. The TM SPP guided wavelength for this free-standing graphene is $\lambda_{SPP} = \lambda_o / 69.34 = 144.22$ nm. This highly compressed mode offers an effective SPP index of $n_{SPP} \equiv \beta_{SPP} / k_o = 69.34$ and has a relatively long propagation length $l_{prop} = 15.6\lambda_{SPP} = 0.225\lambda_o = 2.25\mu$m. In addition to the uniformly biased scenario, we can also engineer the SPP to reflect and refract on the same sheet of graphene by varying the electric bias spatially. To achieve this goal, one may consider three possible methods: 1) A split gate structure to apply different bias voltages to different gates. This is shown schematically in Fig. 2b, in which the potentials V_{b1} and V_{b2}, applied to two gate electrodes, are chosen to provide different chemical potential values of, e.g. $\mu_{c1} = 0.15$ eV and $\mu_{c2} = 0.065$ eV in the two halves of graphene. For sake of clarity, in Fig. 2b and also later in part of Fig.3 the "gate electrodes" are symbolically shown above the graphene at a small distance. In practice, however, the gates are usually located on the substrate beneath the graphene; 2) An *uneven* ground plane, i.e., by

designing the specific profile of the ground plane underneath the dielectric spacer holding the graphene, one can achieve *nonuniform* static biasing electric field under the graphene while the voltage applied between entire sheet of graphene and the ground plane is kept fixed. This is schematically shown in Figs. 3b and 3d (also with more details in Fig S1 and S3). Since in this scenario the separation distance between the graphene and the ground plane is not uniform, the static electric field due to the single bias voltage between the graphene and ground plane is nonuniform, therefore the sheet of graphene experiences different local carrier densities and hence different chemical potentials at different segments; and 3) Inhomogeneous permittivity distribution near the top surface of the spacer holding a sheet of graphene; inhomogeneous distribution of permittivity generates a nonuniform static electric field under the graphene, creating inhomogeneous chemical potential and in turn inhomogeneous conductivity across the graphene (see Fig S2). It is worth to note that with current nanofabrication techniques, it seems that it is straightforward to achieve deeply subwavelength widths for the graphene region with a different conductivity value.

In Fig. 2b, with these bias arrangement the conductivity values of the two segments are, respectively, $\sigma_{g1} = 0.0009(31) + i0.0765(06)$ mS and $\sigma_{g2} = 0.0039(25) - i0.0324(30)$ mS. The "farther" half section with $\sigma_{g1,i} > 0$ supports a TM SPP, while the "closer" half with $\sigma_{g1,i} < 0$ does not. Therefore, if a TM SPP is launched in the farther-half section towards the interface of two sections, it reflects back at that "invisible" boundary line on the same graphene. Figure 2b shows the simulation results which do support this phenomenon. In this scenario the incoming and reflected SPPs are combined to form an oblique standing wave. The reflection of SPP at this line resembles the Fresnel reflection of a plane wave from a planar interface between two media. Here, however, such reflection occurs along an essentially "one-atom-thick" platform, with a

little radiation loss due to the high confinement of SPP to the graphene. This case might also be analogous to the Fresnel reflection from a planar interface between a medium that supports a propagating wave (e.g., a medium with a real refractive index such as a dielectric) and another medium that does not support a propagating wave (e.g., a medium with no real index, such as a noble metal). Accordingly, on the graphene the Fresnel reflection results in a near complete reflection. The simulation results reveal an effective reflection at the boundary "invisible" line between the two segments.

Based on the analogy we just established, we can have a guided IR edge wave along the boundary line between these two sections. The numerical simulations show the presence of such guided IR edge wave, as shown in Fig. 3a. This special guided wave propagates along a "one-atom-radius" boundary line. By post processing the simulation results, we estimate the wavelength of the guided edge wave to be around $\lambda_{edge} = 61.5$ nm. This phenomenon might be relevant, and coupled to, the electronic behavior near the p-n junction edge on the graphene *(18-20)*.

By extending this idea, we propose a setting analogous to a conventional 3D metal-dielectric-metal waveguide, nonetheless on a "one-atom-thick" platform. Figure 3b presents simulation results for such a so-called 2D "metal-dielectric-metal" waveguide, on a "one-atom-thick" graphene. In this case there are three distinct regions on the graphene: two side regions with chemical potential μ_{c2} that have conductivity $\sigma_{g2} = 0.0039(25) - i0.0324(30)$ mS with $\sigma_{g2,i} < 0$, and a middle narrow "ribbon-like" section, with chemical potential μ_{c1} that has conductivity $\sigma_{g1} = 0.0009(31) + i0.0765(06)$ mS where $\sigma_{g1,i} > 0$. The uneven ground plane, schematically shown under the graphene in Fig. 3b, is a proposed method to achieve these two different chemical potentials—however, in the numerical simulation, the graphene is assumed to be free

standing in vacuum, since the SPP is highly confined to the graphene—refer to Fig. S3 for a schematic of the idea of uneven ground plane. A guided SPP wave, bounded by the two boundary lines between the graphene sections, is present, as shown in Fig. 3b. The width of the ribbon-like path is 200 nm. Figure 3c shows a similar structure but with an arbitrarily chosen narrower width of 30 nm, showing that coupled edge wave exists in this ribbon-like "one-atom-thick" waveguide. This scenario may be realized by using an inhomogeneous distribution of permittivity of dielectric spacer (not shown here) under the graphene. This Figure shows that by spatially varying the bias arrangement, we can also bend the ribbon, and still maintain the bounded SPP guided through the bend. Additionally, Figure 3d demonstrates an IR splitter, which can be realized either by employing proper spatial distribution for the bias electric field—which can be achieved by proper design of uneven ground plane—or by applying different bias voltages to electrodes in a split gate scenario. The mechanism for guiding IR signals across the graphene offers exciting possibility for highly miniaturized, "one-atom-thick" photonic nanocircuitry with numerous potential applications in information processing at the nanoscale *(27)*.

Besides the mechanism described above, we can also have "one-atom-thick" scenarios analogous to 3D guided wave propagation in optical fibers with two different dielectric media of different refractive indices as the core and cladding. In other words, the two sections of graphene could be biased to support two TM SPP modes with two distinct effective indexes $n_{SPP,1}$ and $n_{SPP,2}$. We can then realize waveguiding effects similar to those illustrated earlier based on this notion (not shown here for the sake of brevity).

By exploiting the above concepts one can, as well, envisage 2D IR metamaterials and transformation optical devices on a single layer of carbon atoms. In Fig. 4a, we present our

simulation results for the SPP propagation along a layer of graphene within which, an array of two-dimensional (2D) circular "patches" is created. These patches are biased at voltage V_{b2} ($\sigma_{g2} = 0.0039(25) - i0.0324(30)$ mS with $\sigma_{g2,i} < 0$), while the rest of graphene is biased at V_{b1} ($\sigma_{g1} = 0.0009(31) + i0.0765(06)$ mS with $\sigma_{g1,i} > 0$). We note that each circular patch acts a scatterer for the SPP surface wave, behaving as a "one-atom-thick" "flatland inclusion". The collection of these "inclusions" creates a 2D bulk flat metamaterials. The SPP interaction in a two-dimensional IR metamaterial is demonstrated in the simulation results shown in Fig. 4a. This numerical demonstration verifies that the proposed geometry may indeed be designed to be the 2D analog of the 3D metamaterials formed by collections of subwavelength metallic nanoparticles—metamaterials that can exhibit backward wave propagation *(28)*.

Furthermore, an example of an IR transformation optical device is presented in Fig. 4b. A "flat" version of a Luneburg lens is designed on the graphene by creating several concentric rings with specific conductivity values. These values may be obtained either by applying a proper set of bias voltages, by properly designing the uneven ground plane, or by fabricating inhomogeneous spacer permittivity. For instance, with a special configuration of bias arrangement, we can create, approximately, a graded conductivity pattern that provides the required effective SPP graded index for operation of the Luneburg lens. To find the corresponding conductivities for these concentric rings we use the discretised approximate expression $\sigma_{i,n} = \sigma_{i,out}\left[2 - \left(r_n + r_{n-1}\right)^2 / 4\right]^{-1/2}$ where $\sigma_{i,n}$ and r_n are, respectively, the imaginary part of conductivity and radius of the *n*th section and $\sigma_{i,out}$ is the imaginary part of conductivity of the "background" graphene on which the lens is created. As our simulation results in Fig. 4b reveal, the SPP generated from a "point-like" source is evolved into an approximately "one-atom-thick

collimated beam" of SPP on the graphene, as analogously a conventional 3D Luneburg lens acts for a 3D beam. The diameter of the "flat" Luneburg lens in our simulation is about $1.5\ \mu$m, which is $0.15\lambda_o$—a notably subwavelength size. This example suggests that one can design various subwavelength IR devices (e.g., convex lens, concave lens, etc) on the graphene—a versatile platform for nanoscale Fourier optics *(27)* and other photonic signal processing methods.

Finally, a flat version of the "superlensing" effect *(29-30)* is shown in Fig. 4c. In this simulation, an IR source on a graphene, biased at voltage V_{b1} (equivalently chemical potential μ_{c1}), is situated near a "strip" region of graphene biased at V_{b2} (or μ_{c2}). With proper choice of biases (resulting in a required set of conductivity values for the strip and the region outside the strip) and proper adjustment of width of the strip and separation between the source and the strip, we can implement an approximate superlensing effect, as our simulation results verify this possibility.

In conclusion, our theoretical study of IR wave interaction with graphene suggests that the graphene can be used as a low-loss "one-atom-thick" platform for flatland IR metamaterials and transformative optics. The required inhomogeneous, nonuniform patterning of conductivity may be achieved by various techniques such as varying chemical potentials, creating uneven ground plane, fabricating inhomogeneous permittivity of spacer dielectric, applying gate electric or magnetic field, and/or utilizing heated atomic force microscopy technique to reduce oxide of a graphene oxide sheet *(21)*. This unique platform opens new vistas in nanoscale and microscale photonic information processing and photonic circuitry.

References:

[1] W. Cai, and V. Shalaev, V., *Optical Metamaterials: Fundamentals and Applications*, Springer, New York (2010).

[2] D. R. Smith, J. B. Pendry, M. C. K., Wiltshire, *Science* **305**, 788 (2004)

[3] N. Engheta, and R. W. Ziolkowski, *Metamaterials, Physics and Engineering Explorations*, IEEE-Wiley, New York (2006).

[4] G. V. Eleftheriades, and K. G. Balmain, *Negative-Refractionn Metamaterials,* IEEE, New York (2005).

[5] J. B. Pendry, D. Schurig, and D. R. Smith, *Science* **312**, 1780 (2006).

[6] D. Schurig, J. J. Mock, B. J. Justice, S. A. Cummer, J. B. Pendry, A. F. Starr, D. R. Smith, *Science* **314**, 977 (2006).

[7] U. Leonhardt, *Science* **312**, 1777 (2006).

[8] S. Maier, *Plasmonics: Fundamentals and Applications*, Springer, New York (2007).

[9] K. S. Novoselov, A. G. Geim, S. V. Morozov, D. Jiang, M. I. Katsnelson, I. V. Grigorieva, S. V. Dubonos, and A. A. Firsov, *Nature* (London) **438**, 197 (2005).

[10] A. K. Geim, and K. S. Novoselov, *Nature Materials*. **6**, 183 (2007).

[11] V. P. Gusynin, S. G. Sharapov, and J. P. Carbotte, *J. Phys.: Condens. Matter*, **19**, 026222 (2007).

[12] V. P. Gusynin, and S. G. Sharapov, *Phys. Rev. B.*, **73**, 245411 (2006).

[13] G. W. Hanson, *Journal of Applied Physics*, **103**, 064302 (2008).

[14] S. A. Mikhailov, and K. Ziegler, K., *Physical Review Letters*, **99**, 016803 (2007).

[15] D. R. Anderson, *J. Opt. Soc. Am. B.* 27(4), 818 (2010)

[16] M. Jablan, H. Buljan, and M. Soljacic, *Physical Review B*, **80**, 245435 (2009).

[17] F. Rana, *IEEE Trans. Nanotechnology*, 7(1), 91 (2008).

[18] E. G. Mishchenko, A. V. Shytov, A. V., and P. G. Silvestrov, *Phys. Rev. Lett.*, 104, 156806 (2010)

[19] V. V. Cheianov, V. Fal'ko, and B. L. Altshuler, *Science*, Vol. 315, p. 1252 (2007)

[20] R. Dehbashi, D. Fathi, S. Mohajerzadeh, and B. Forouzandeh, *IEEE J. Selected Topics in Quantum Electronics*, 16(2), 394 (2010).

[21] Z. Wei, Z., *et al. Science* 328, 1373 (2010).

[22] E. H. Hwang, and S.Das Sarma, *Rev. B.*, **75**, 205418 (2007)

[23] P. R. West, *et al. Laser and Photonics Review*, 1-13 (2010)

[24] N. Papasimakis, *et al.*, *Optics Express*, 18(8), 8353 (2010)

[25] A. Alu and N. Engheta, *Journal of Optical Society of America B*, 23, 571 (2006)

[26] E. D. Palik, *Handbook of Optical Constants of Solids I* Academic Press, Orlando, Florida, 353- 357 (1985).

[27] N. Engheta, *Science* **317**, 1698 (2007).

[28] Alu, A., and Engheta, N., *Physical Review B.*, **75**, 024304 (2007)

[29] J. B. Pendry, *Physical Review Letters*, **85**, 3966 (2000).

[30] N. Fang, H., Lee, C. Sun, X. Zhang, *Science* **308**, 534 (2005).

[31] CST Studio Suite 2010. <www.cst.com>

Acknowledgements

This work is supported in part by the US Air Force Office of Scientific Research (AFOSR) grant number FA9550-08-1-0220.

Figures:

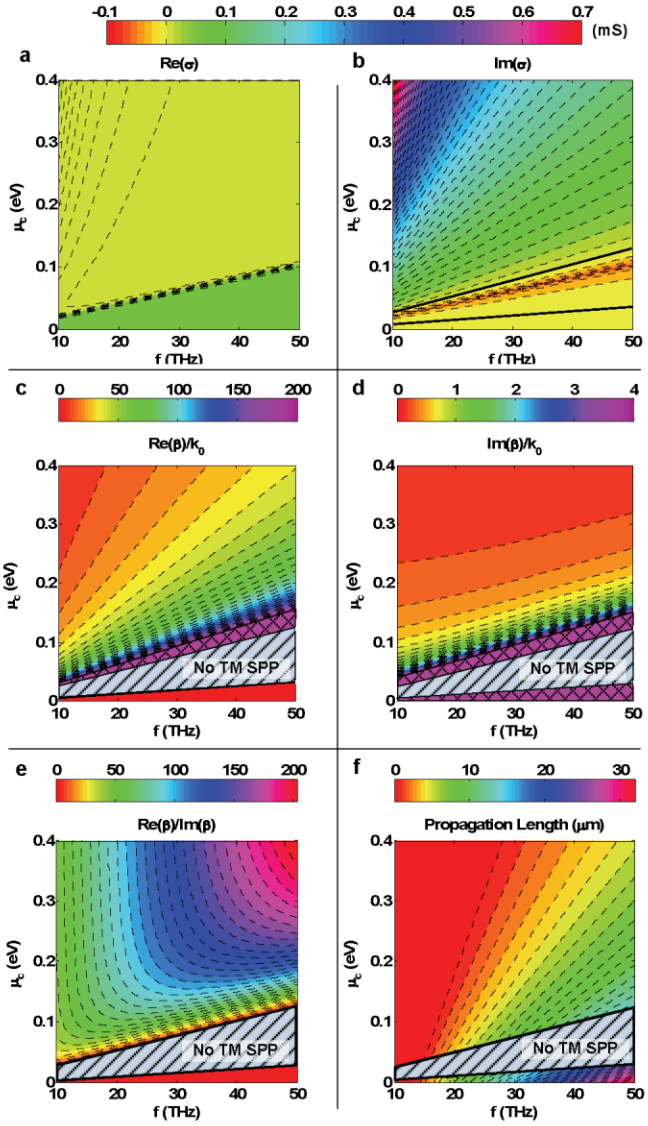

Fig. 1. Graphene conductivity and characteristics of the transverse-magnetic (TM) SPP surface waves. (**A**) Real part of the conductivity of a free-standing Graphene as a function of chemical potential μ_c and the frequency f, according to Kubo formula *(12, 14)* for $T = 3\text{K}$, $\Gamma = 0.43\,\text{meV}$. (**B**) Imaginary part of the conductivity for the same graphene sheet. **c**, Real part of the wave number β of the TM SPP supported by the graphene with the same parameters mentioned in (**A**) and (**B**)—The purple cross-hatched area is corresponding to $\text{Re}(\beta) \geq 200k_0$.

(**D**) Imaginary part of the wave number β of the TM SPP supported by the same graphene layer mentioned in (**A**) and (**B**). When $\mathrm{Im}(\sigma_g) < 0$, no TM SPP is supported—The purple cross-hatched areas are corresponding to $\mathrm{Im}(\beta) \geq 4k_0$. (**E**) The "figure-of-merit", defined as $\mathrm{Re}(\beta)/\mathrm{Im}(\beta)$, for the SPP mode as a function of μ_c and f. (**F**) The propagation length of the SPP mode, defined as $1/\mathrm{Im}(\beta)$.

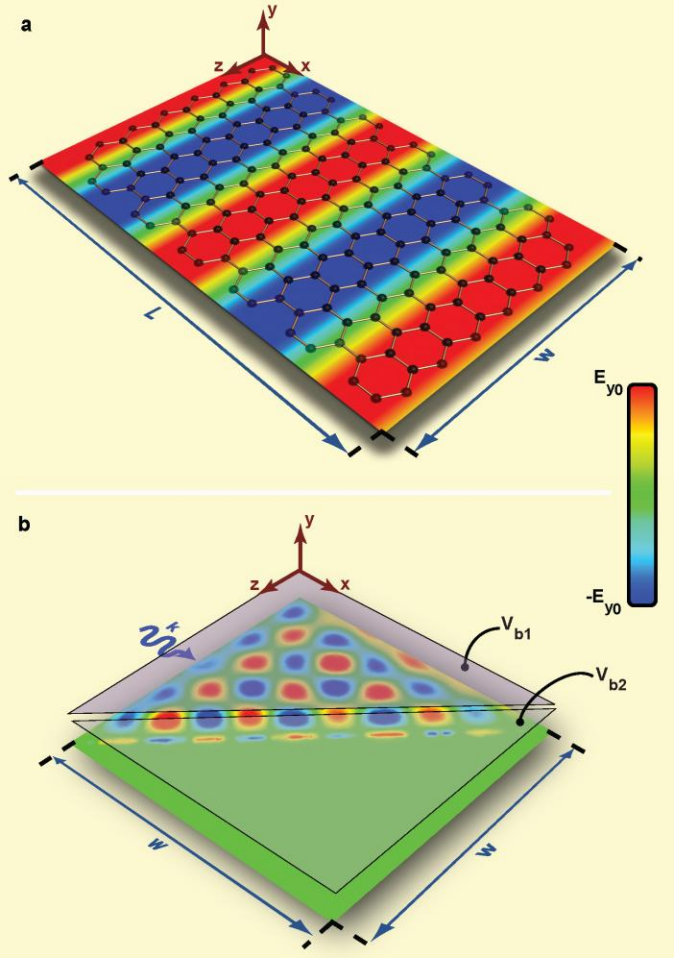

Fig. 2. (**A**) Simulation results showing the y-component of the electric field, E_y, for a TM SPP mode at 30 THz guided by a uniformly biased graphene layer with dimensions $L = 350$ nm, $w = 235$ nm ($T = 3\,\mathrm{K}$, $\Gamma = 0.43$ meV, $\mu_c = 0.15$ eV across the entire graphene). This chemical potential can be achieved, for example, by a bias voltage of 22.84 V across a 300-

nm SiO_2 spacer between the graphene and the Si substrate (but Si substrate and SiO2 spacer are not considered here). The SPP wavelength along the graphene, λ_{SPP} is much smaller than free-space wavelength λ_o, i.e., $\lambda_{SPP} = 0.0144\lambda_o$. (**B**) Simulation results of the E_y for the near total reflection of a TM SPP on a sheet of graphene with side $w = 800$ nm; two different gate bias voltages are applied. The V_{b1} and V_{b2} are chosen to provide different chemical potential values of $\mu_{c1} = 0.15$ eV and $\mu_{c2} = 0.065$ eV in the two halves of graphene (corresponding complex conductivity values are $\sigma_{g1} = 0.0009(31) + i0.0765(06)$ mS and $\sigma_{g2} = 0.0039(25) - i0.0324(30)$ mS). Section 1 supports a TM SPP, while Section 2 does not; see the text for complete explanation of this effect.

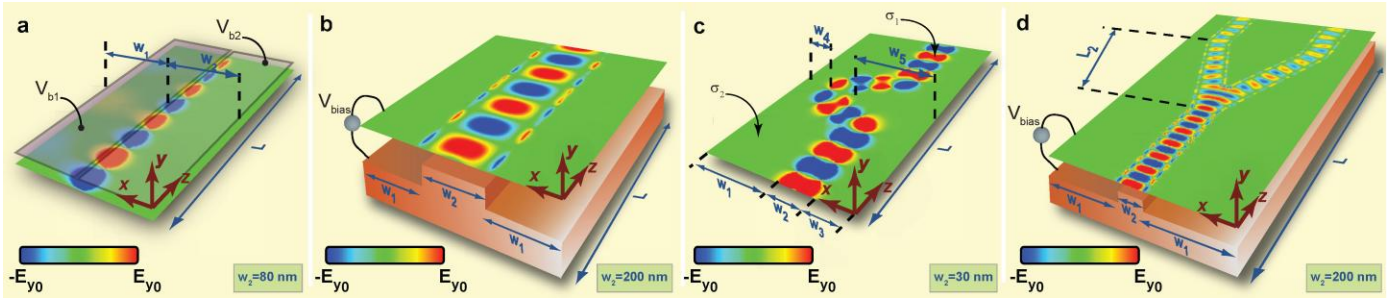

Fig. 3. (**A**) Distribution of E_y (snap shot in time) of a guided IR edge wave at $f = 30\,THz$, supported along the boundary line between the two sections of the same sheet of graphene, which has two different conductivity regions, as in Fig. 2b ($L = 250$ nm and $w = 80$ nm). (**B**) Simulation results of E_y (snap shot in time) for an IR guided wave at $f = 30\,THz$ along the ribbon-like section of graphene with the chemical potential μ_{c1}, which may be achieved by heightening the ground plane underneath this region. The corresponding graphene conductivity of the ribbon is $\sigma_{g1} = 0.0009(31) + i0.0765(06)$ mS. This ribbon-like path is surrounded by the

two other sections of graphene with chemical potential μ_{c2}, which may be obtained by reducing the height of the ground plane beneath these regions. The corresponding graphene conductivity is $\sigma_{g2} = 0.0039(25) - 0.0324(30)$ mS). The IR signal is clearly guided along this "one-atom-thick" ribbon. The computational region has the length $L = 560$ nm and total width $(W_1 + W_2 + W_3) = (120 + 120 + 120)$ nm. (**C**) Similar to panel b, but with the ribbon width of 30 nm, arbitrarily chosen to demonstrate the effects of coupling of two edge waves, providing another waveguiding phenomenon along this ribbon and also showing the bending effect. The computational region has the length $L = 370$ nm and total width $(W_1 + W_2 + W_3) = (120 + 30 + 60)$ nm while for the bent region $(W_4 + W_2 + W_5) = (30 + 30 + 120)$ nm. (**D**) Similar to panel b, but with the ribbon-like section split into two paths ($L_2 = 1077$ nm). The splitting of the SPP along this one-atom-thick structure is clearly seen in this simulation. The computational region shown has the length $L_1 = 2540$ nm and total width $(W_1 + W_2 + W_3) = (600 + 200 + 600)$ nm. Note different scale bars in different panels.

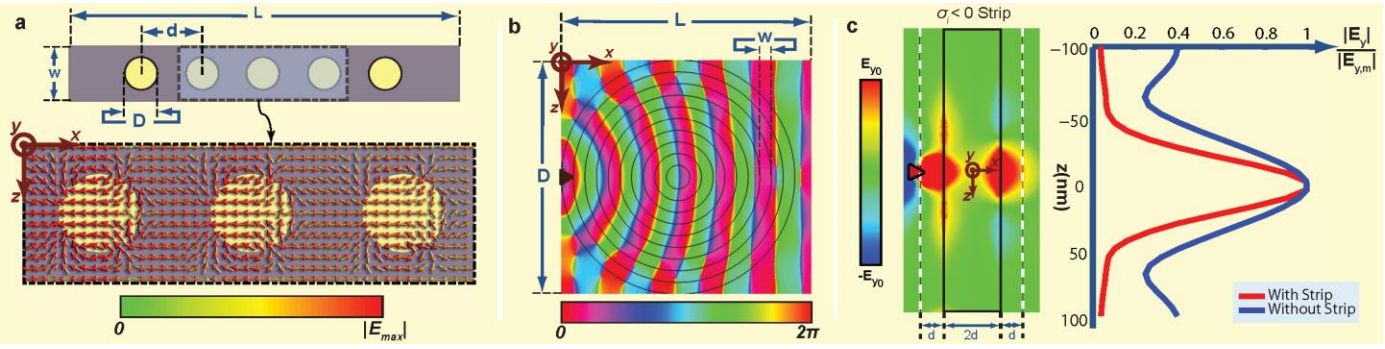

Fig. 4 (**A**) Flatland Metamaterials: the snap shot in time of the electric field vectors for the SPP at $f = 30$ THz, shown on the x-z plane of the graphene, on which a 2D array of subwavelength circular patches is assumed. The patches conductivity is σ_{g2}, where $\mathrm{Im}(\sigma_{g2}) < 0$. The rest of

the graphene has the conductivity σ_{g1} with $\mathrm{Im}(\sigma_{g1}) > 0$. Only one row of the 2D periodic array is shown ($D = 30$ nm, $d = w = 55$ nm, $L = 370$ nm). Scattering of the SPP from these patches along the graphene leads to a bulk SPP property, yielding a flatland IR metamaterial. (**B**) Flatland Luneburg lens: Simulation results for the phase of E_y of the SPP at $f = 30\,THz$ along the graphene, on which ten concentric annular regions with required conductivity values, according to Luneburg lens expression, are produced ($D = 1.5$ μm nm, $w = 75$ nm, $L = 1.6$ μm). Simulation results indicate such "one-atom-thick" Luneburg lens indeed collimates the SPP. (**C**) Flatland "superlens": Simulation results for E_y of SPP at $f = 30\,THz$ on the graphene with a subwavelength strip region with conductivity σ_{g2}, while the rest of graphene has the conductivity σ_{g1}. The object—a point source—and image planes are assumed to be respectively 10 nmaway from the left and right edges of the strip ($w = 2d = 20$ nm). The normalized intensity of E_y at the image plane is shown for two cases with and without the strip (Normalization is with respect to their respective peak values). The subwavelength "focusing" is observable due to presence of the strip with conductivity σ_{g2} — $\mathrm{Im}(\sigma_{g2}) < 0$.

Supporting Material

Methods

We have used commercially available full-wave electromagnetic simulator software, CST Studio Suite *(31)* in order to obtain the 3D numerical simulations presented in Figs 2, 3 and 4. For the purpose of our 3D simulation, the thickness of graphene is assumed to be 1 nm, although other extremely small values for this thickness lead to similar results. (We have assumed 1 nm thickness for graphene and assigned the corresponding permittivity in our simulations. Note that as long as the chosen thickness is extremely small compared to the wavelength, this particular choice is not essential—we could assume thickness of 0.5 nm and find the corresponding permittivity value.) Due to the large difference in the dimensions of the graphene layer (thickness vs. width and length), and also due to the special form of the conductivity function of graphene, we have chosen frequency-domain Finite Element Method (FEM) solver of CST. This solver solves the problem for a single frequency at a time. For each frequency sample, the linear equation system is solved by an iterative solver. Adaptive tetrahedral meshing with a minimum feature resolution of 0.5 nm has been used in the simulations. A point source (equivalent of an infinitesimal dipole antenna) has been utilized as the excitation of the structures. All the simulations reached proper convergence; a residual energy of 10^{-5} of its peak value has been obtained in the computation region. In order to absorb all the energy and to have approximately zero-reflection boundary, on the receiving side, in all the simulations a technique similar to the well-known Salisbury Shield method has been implemented (with proper modifications for a TM SPP mode). Depending on the nature of the problem, perfect magnetic conducting (PMC), perfect electric conducting (PEC) and open boundary conditions have been applied to different boundaries, to mimic the two-dimensionality of the geometry.

Figures

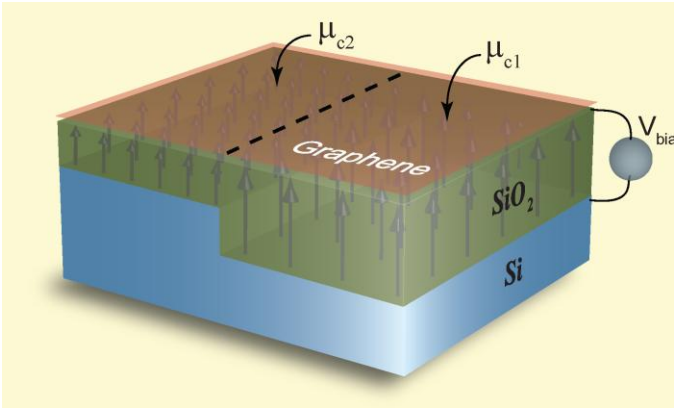

Fig. S1. Schematic of the idea of *uneven* ground plane underneath the graphene layer in order to construct inhomogeneous conductivity pattern across a single flake of graphene. By biasing the graphene with a single static voltage, the static electric field is distributed according to the height of the spacer between the graphene and the uneven ground plane, leading to the unequal static electric field. This results in unequal carrier densities and chemical potentials μ_{c1} and μ_{c2} on the surface of the single graphene and thus different conductivity distributions across the graphene.

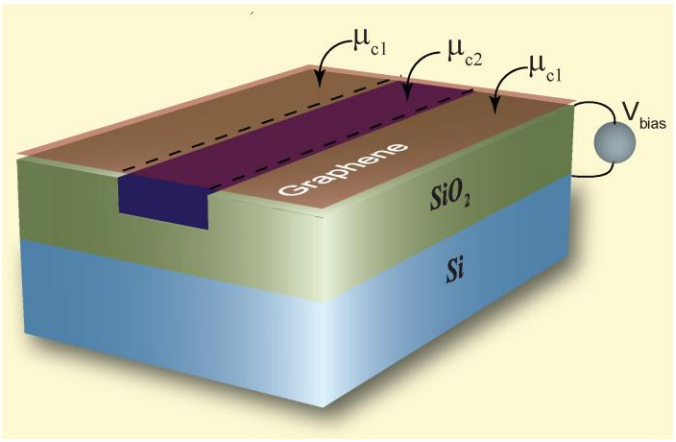

Fig. S2. Sketch of another idea to create inhomogeneous conductivity across a single sheet of graphene. Here several dielectric spacers with unequal permittivity functions are assumed to be used underneath of the graphene. This can lead to unequal static electric field distributions, resulting in inhomogeneous conductivity patterns across a single sheet of graphene.

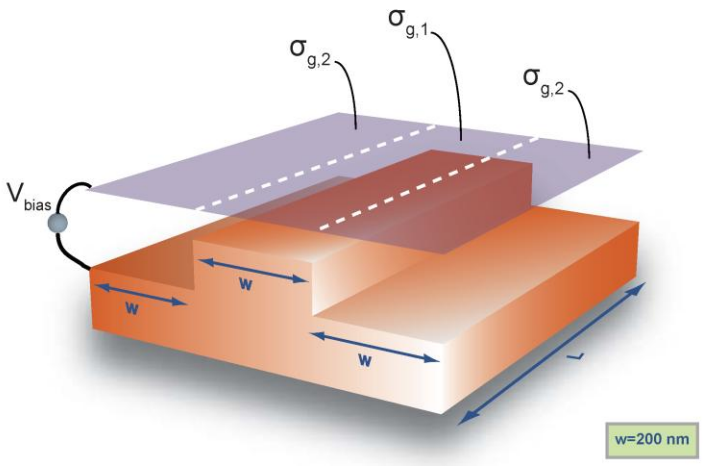

Fig. S3. Another schematic of the uneven ground plane idea to create inhomogeneous conductivity across a single sheet of graphene. This idea is also sketched in our Fig. 3.

CST视频培训课程推荐

CST 微波工作室(CST Microwave Studio)是 CST 工作室套装中最核心的一个子软件，主要用于三维电磁问题的仿真分析，可计算任意结构任意材料电大宽带的电磁问题。广泛应用于高频/微波无源器件的仿真设计、各种类型的天线设计、雷达散射截面分析、电磁兼容分析和信号完整性分析等各个方面。

易迪拓培训(www.edatop.com)推出的 CST 微波工作室视频培训课程由经验丰富的专家授课，旨在帮助用户能够快速地学习掌握 CST 微波工作室的各项功能、使用操作和工程应用。购买 CST 教学视频培训课程套装，还可超值赠送 3 个月免费在线学习答疑，让您学习无忧。

CST 学习培训课程套装

该培训套装由易迪拓培训联合微波 EDA 网共同推出，是最全面、系统、专业的 CST 微波工作室培训课程套装，所有课程都由经验丰富的专家授课，视频教学，可以帮助您从零开始，全面系统地学习 CST 微波工作的各项功能及其在微波射频、天线设计等领域的设计应用。且购买该套装，还可超值赠送 3 个月免费学习答疑…

课程网址：http://www.edatop.com/peixun/cst/24.html

HFSS 天线设计培训课程套装

套装共含 5 门视频培训课程，课程从基础讲起，内容由浅入深，理论介绍和实际操作讲解相结合，全面系统的讲解了 CST 微波工作室天线设计的全过程。是国内最全面、最专业的 CST 天线设计课程，可以帮助您快速学习掌握如何使用 CST 设计天线，让天线设计不再难…

课程网址：http://www.edatop.com/peixun/cst/127.html

更多 CST 视频培训课程：

- **CST 微波工作室入门与应用详解 — 中文视频教程**
  CST 微波工作室初学者的最佳培训课程，由工程经验丰富的资深专家授课，全程中文讲解，高清视频，直观易学。网址：http://www.edatop.com/peixun/cst/25.html
- **CST 微波工作室天线设计详解 — 中文视频培训教程**
  重点讲解天线设计相关知识和使用 CST 进行天线仿真设计的使用操作，是学习掌握使用 CST 微波工作室进行天线设计的必备课程，网址：http://www.edatop.com/peixun/cst/26.html
- **CST 阵列天线仿真设计实例详解 —— 中文视频教程**
  阵列天线设计专业性要求很高，因此相关培训课程是少之又少，该门培训课程由易迪拓培训重金聘请专家讲解；课程网址：http://www.edatop.com/peixun/cst/123.html
- **更多 CST 培训课程**，敬请浏览：http://www.edatop.com/peixun/cst

关于易迪拓培训：

易迪拓培训(www.edatop.com)由数名来自于研发第一线的资深工程师发起成立，一直致力和专注于微波、射频、天线设计研发人才的培养；后于 2006 年整合合并微波 EDA 网(www.mweda.com)，现已发展成为国内最大的微波射频和天线设计人才培养基地，成功推出多套微波射频以及天线设计相关培训课程和 ADS、HFSS 等专业软件使用培训课程，广受客户好评；并先后与人民邮电出版社、电子工业出版社合作出版了多本专业图书，帮助数万名工程师提升了专业技术能力。客户遍布中兴通讯、研通高频、埃威航电、国人通信等多家国内知名公司，以及台湾工业技术研究院、永业科技、全一电子等多家台湾地区企业。

我们的课程优势：

※ 成立于 2004 年，10 多年丰富的行业经验

※ 一直专注于微波射频和天线设计工程师的培养，更了解该行业对人才的要求

※ 视频课程、既能达到现场培训的效果，又能免除您舟车劳顿的辛苦，学习工作两不误

※ 经验丰富的一线资深工程师讲授，结合实际工程案例，直观、实用、易学

联系我们：

※ 易迪拓培训官网：http://www.edatop.com

※ 微波 EDA 网：http://www.mweda.com

※ 官方淘宝店：http://shop36920890.taobao.com